RSC Advances

PAPER

Cite this: *RSC Adv.*, 2016, **6**, 102015

Alkaline niobates $ANbO_3$ (A = Li, Na, K) as heterogeneous catalysts for dipropyl sulfide oxidation†

Candelaria Leal Marchena,*[a] Clara Saux,[a] Robinson Dinamarca,[b] Gina Pecchi[b] and Liliana Pierella[a]

Received 30th August 2016
Accepted 19th October 2016

DOI: 10.1039/c6ra21749d

www.rsc.org/advances

Alkaline $ANbO_3$ (A = Li, Na, K) niobates with perovskite-type structure were prepared by a sol gel method, characterized by XRD, BET, TG/DTA, O_2-TPD, DRS UV-Vis and FTIR and evaluated as heterogeneous catalysts for the selective oxidation of dipropyl sulfide (DPS) to its corresponding sulfoxide. The effects of different reaction parameters were evaluated, such as catalyst weight, the solvent and oxidant nature, reaction temperature and reuse. In order to gain better knowledge of the oxidation process, a kinetic study of the reaction was carried out. The global pseudo first order constant, the initial reaction rate and the apparent activation energy were calculated, and simplified reaction steps are proposed. $KNbO_3$ showed the highest catalytic activity and sulfoxide selectivity with a periodic trend of $KNbO_3$ > $NaNbO_3$ ~ $LiNbO_3$.

1. Introduction

Perovskites are interesting inorganic structures, whose general chemical formula is typically ABX_3, where A and B are cations of dissimilar sizes (the larger A-site usually is a rare earth metal and the B-site a first row transition metal) and X is an anion binding to both. Although this general formula is relatively simple, it hides an exceptional diversity of atomic arrangements. When X anion is oxygen, these materials are called oxide perovskites and have been actively studied for their ferroelectric, magnetic, piezoelectric, magnetoresistive and superconductive properties.[1] For alkaline metals in the A-site, the charge balance to meet the perovskite structure is satisfied with vanadium(v) and niobium(v) at the B-site.[2] Lithium niobate ($LiNbO_3$), sodium niobate ($NaNbO_3$) and potassium niobate ($KNbO_3$), well-known as alkaline niobates, have been reported with interesting applications such as piezoelectricity, pyroelectricity, electro-optic, and nonlinear optical behavior.[3] Moreover, interesting catalytic properties have also been reported,[4,5] closely related to the atomic number of the metal.[6,7] Lithium niobate is a well-known and transparent semiconductor with important technological applications mainly in solid-state based optical devices, such as optical modulators, in either bulk or nanostructured forms.[6,8] Potassium niobate has also been widely reported as an interesting material for optical and photocatalytic applications.[9] Moreover, $KNbO_3$ and $NaNbO_3$ have been identified as promising alternatives to currently used piezoelectric ceramics, mainly based on lead zirconate titanate. However, their use or the use of other niobates as catalysts in the selective oxidation of sulfides has been scarcely reported in literature.[10,11] It have been reported in literature for sulfoxidation reactions employing mild oxidizing agents, the use of homogeneous catalyst, such as $HAuCl_4 \cdot 4H_2O$,[12] Mo(vi) salts,[13] and heterogeneous catalysts, such as, MoO_3;[14] dioxo-molybdenum(vi) complex;[15] heterogeneous TiO_2;[16] tantalum(v) and niobium(v);[17] composite oxide catalyst $LiNbMoO_6$,[18] among others.

The chemistry of organic sulfur-containing compounds has been widely reported due to presence of sulfoxides and other sulfur compounds as important intermediates in several pharmaceutical and fine chemistry reactions.[19,20] The well-known omeprazole medicine and the fipronil pesticide are, among others, two typical examples of the extensive applications of these intermediates.[21,22] Sulfoxides are generally prepared *via* oxidation of the corresponding sulfides using stoichiometric amounts of organic[23,24] or inorganic reagents.[25,26] Sulfide oxidation does not only have applications in sulfoxide or sulfone synthesis, since they can also be harnessed in decontamination processes, as sulfoxides are less toxic than the corresponding sulfides.[27] Most of these experimental procedures are expensive, require drastic conditions, extended reaction times and low yields of the desired products are obtained. The use of "green oxidants" such as molecular oxygen or hydrogen peroxide in the sulfide to sulfoxide reaction is a very attractive, as these oxidants are readily available, inexpensive and environmentally benign with the formation of water as the only by-product.

[a]*Centro de Investigación y Tecnología Química (CITeQ), UTN – CONICET, Maestro Marcelo López esq. Cruz Roja, (5016) Córdoba, Argentina. E-mail: cleal@frc.utn.edu.ar; Fax: +54 351 4690585; Tel: +54 351 4690585*

[b]*Department of Physical Chemistry, University of Concepción, Concepción, Chile*

† Electronic supplementary information (ESI) available: Supporting figure of the oxygen desorption profiles of $ANbO_3$ (A = Li, Na, K) niobates (Fig. S1). See DOI: 10.1039/c6ra21749d

This oxidation reaction employing hydrogen peroxide as oxidant has been shown to be one of the most attractive methods; however, the reaction rates are slow, therefore, to improve on this method, further studies have been undertaken.[28–30]

In light of the above, we hypothesize that with the advantages of the perovskite-type structure of alkaline niobates, it would be possible to obtain active heterogeneous catalysts for sulfide oxidation. To better understand the different activities of the alkaline niobates and to identify the key-parameters involved in the catalytic oxidation of sulfides employing alkaline niobates with the perovskite structure, we present in this article Li, Na and K niobates that have been prepared, characterized and evaluated for the selective oxidation of dipropyl sulfide. The global pseudo first order constant, the initial reaction rate and the apparent activation energy are also determined.

2. Experimental

2.1. Alkaline niobates synthesis

Alkaline niobates ($LiNbO_3$, $NaNbO_3$ and $KNbO_3$) were prepared following the procedure reported by Wang *et al.*,[31] employing the corresponding alkaline acetates, hydrogen peroxide (H_2O_2) and citric acid as starting materials. An aqueous solution of the alkaline acetate was mixed at room temperature with a stoichiometric amount of $NbCl_5$ previously dissolved in H_2O_2 under constant stirring. Citric acid was added under constant stirring in a molar ratio of 3 of citric acid to metal cations. The solution was further heated to 80 °C until gels were formed. Finally, the gels were dried at 60 °C for 15 h and then were calcined at 600 °C for 10 h.

2.2. Characterization

X-ray powder diffraction (XRD) patterns were obtained employing a Rigaku diffractometer with Ni-filtered CuKα radiation (λ = 1.5418 Å). Specific areas were determined using the BET method from the nitrogen adsorption isotherms at 77 K on a Micromeritics apparatus model ASAP 2010. The differential thermogravimetry (DTA/TG) experiments of the solids were carried out using a Netzsch 409 PC equipment. The thermogravimetric analyses were performed in a 11% O_2/He gas mixture using a constant sample weight of 40 mg for all experiments. The studied temperature range was 20–1000 °C. Temperature-programmed desorption of oxygen (O_2-TPD) experiments were performed in a TPR/TPD 2900 Micromeritics system with a thermal conductivity detector. The samples were exposed to oxygen for 1 h at 700 °C and then, were cooled at 20 °C. The atmosphere was changed to a helium flow and the sample was heated at a constant rate of 10 °C min^{-1}, and the desorbed oxygen was monitored with a thermal conductivity detector. The oxygen desorbed TPD-MS experiments confirm that the evolved gas and the helium flow only contain oxygen. The diffuse reflectance spectra (DRS UV-Vis) of the materials were recorded using a UV-visible JASCO V 650 spectrophotometer, to which a diffuse reflectance chamber with a 50 mm diameter integrating sphere and internal Spectralon coating is attached, in the 200–800 nm wavelength range. Fourier-transform IR spectra (FTIR) were recorded in a Nicolet Magna-IR 550 instrument equipped with a quartz sample holder with KBr windows. The niobates were mixed with KBr to obtain a niobate–KBr ratio of 1/150.

2.3. Catalytic activity

The catalytic selective oxidation of dipropyl sulfide (DPS) (97%, Sigma-Aldrich) was carried out in a glass flask reactor (25 cm^3) with magnetic stirring immersed in a thermostated bath, equipped with a reflux condenser using a substrate/oxidant molar ratio (R) of 1. The catalytic tests were performed by evaluating different reaction conditions such as: reaction temperature, weight of catalyst, nature of the oxidizing agent (H_2O_2 and *tert*-butyl hydroperoxide) and nature of the solvent (acetonitrile (99.5%, Cicarelli), acetone (analytical grade, Aldrich), 2-propanol (99.5%, Aldrich), methanol (99.5%, Cicarelli), ethanol (99.5%, Cicarelli), 2-butanol (99.5%, Merck) and *n*-hexane (97%, Riedel de Haën)). Blanck experiments were carried out under the same reaction conditions but without catalyst in the reaction mixture. The reactions were monitored by taking aliquots of the reaction mixture at different reaction times. Prior to analysis, the catalyst was separated by filtration. Organic compounds were analyzed quantitatively by gas chromatography (Hewlett Packard HP-5890) with a methyl silicone capillary column (30 m × 0.32 mm i.d.) and a flame ionization detector (FID) and qualitatively by mass spectrometry GC-Mass (Shimadzu QP 5050 GC-17 A) using a HP-S (25 m × 0.2 mm i.d.) capillary column.

3. Results and discussion

3.1. Characterization

In order to identify crystalline phases in the synthesized materials, the X-ray diffraction patterns of the prepared materials are shown in Fig. 1. A rhombohedral structure with hexagonal axis (JCPDS 20-631) for $LiNbO_3$ (ref. 32) can be observed, and for $KNbO_3$, an orthorhombic perovskite-type structure (JCPDS 32-822) is noted with presence of $K_2Nb_{16}O_{41}$ (JCPDS 14-287)[33] as segregated phase. On the other hand, for $NaNbO_3$ the

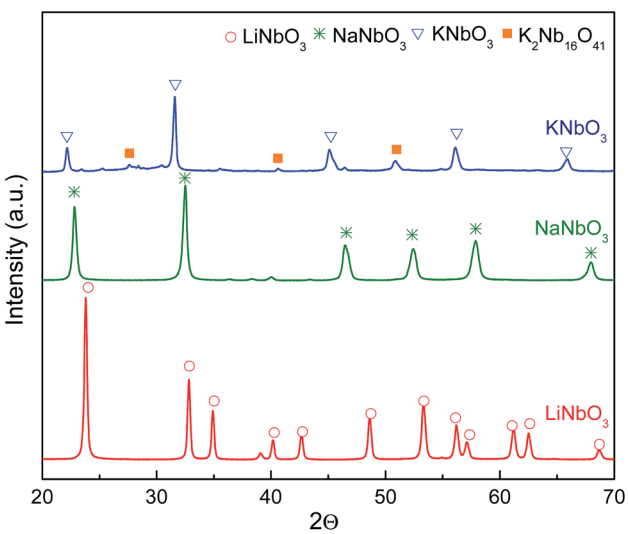

Fig. 1 X-ray diffraction patterns of $ANbO_3$ (A = Li, Na, K) niobates.

diffraction profile corresponds to a single-phase orthorhombic perovskite-type structure (JCPDS 82-606).[34]

For the main phase in each sample, the crystallite size was determined by the Scherrer's formula ($d = K\lambda/B\cos\theta$), where d is the average size of the particles (considering spherical particles), K is a dimensionless shape factor with a value of 0.9, λ is the wavelength of X-ray radiation, B is the full width at half maximum of the diffracted peak and θ is the angle of diffraction. The obtained results, using the 2θ value of 42.5° ($LiNbO_3$) and 58° ($NaNbO_3$ and $KNbO_3$) to calculate the crystallite size, are presented in Table 1. As it can be observed, lower and similar crystal sizes were obtained for $NaNbO_3$ and $KNbO_3$ and larger value for $LiNbO_3$.

In Table 1 it is also reported the crystalline phases and the surface area obtained from nitrogen desorption isotherms. The lower S_{BET} values show not a clear trend and are the expected values for these types of crystalline structures.[35,36]

Fig. 2 shows the TG/DTG profiles of the prepared niobates from 25 °C to 650 °C. Although they were performed up to 1000 °C, no further changes were observed at higher temperatures, indicative of the crystallization of $LiNbO_3$, $NaNbO_3$ and $KNbO_3$ structure[26] also confirmed by XRD. Similar weight loss can be observed for all samples, and to identify the evolved products the evolution of 14, 18, 28, 32, 44 and 46 amu were followed by mass spectrometry (MS). The first weight loss about 3% between 30–100 °C corresponds to the removal of solvent in the samples and the second of approximately 60% below 200 °C to the loss of the free and bound water.[37] At 340 °C corresponds the decomposition of the metal carboxylate gels and the final weight loss, between 400 °C and 500 °C, is assigned to the decomposition of residual organic groups.[38]

Considering that oxygen availability could improve DPS oxidation, O_2-TPD patterns of the solids were also carried out (Fig. S1†). The alkaline niobates present only one broad oxygen desorption peak around 60 °C that could be ascribed to oxygen physically adsorbed on the surface.[39] Physisorption implies a weak oxygen bond to the surface, and in order to optimize this property, the catalytic reaction temperature was fixed around this value. Due to TPD-MS experiments confirm that the evolved gas in the He flow only contains oxygen, it was possible to calculate the amount of oxygen desorbed for each niobate up to 200 °C from O_2-TPD profiles (Table 2). Thus, an increase in the desorbed oxygen can be observed with the increase of the atomic number; and a large amount of desorbed oxygen could be associated with a larger catalytic activity.

The coordination geometry and the chemical arrangement of the Nb species in the prepared niobates were evaluated by DRS UV-Vis spectroscopy. In Fig. 3 a clear maximum excitation at 260 nm, characteristic of the intrinsic niobate group, followed

Table 1 Specific area, detected crystalline phases and crystal size for $ANbO_3$ (A = Li, Na, K) niobates

Catalysts	S_{BET} ($m^2\ g^{-1}$)	Crystalline phases		d (nm)
$LiNbO_3$	13	Hexagonal rhombohedral	$LiNbO_3$	40
$NaNbO_3$	17	Orthorhombic	$NaNbO_3$	18
$KNbO_3$	10	Orthorhombic	$KNbO_3$ $K_2Nb_{16}O_{41}$	17

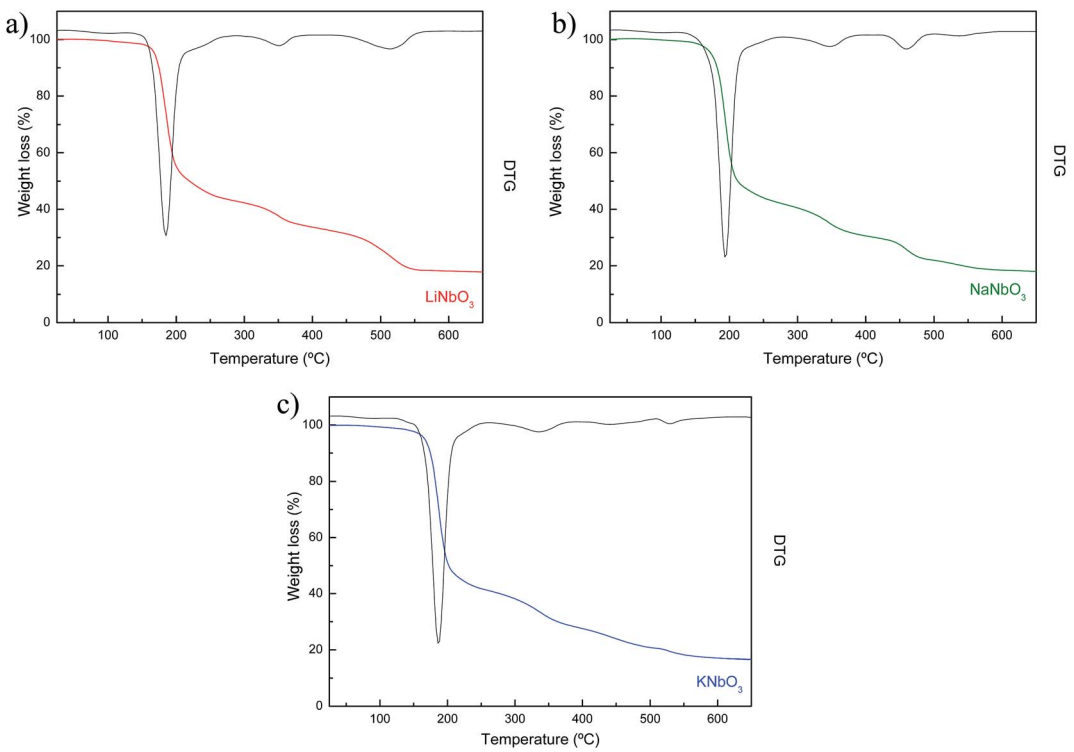

Fig. 2 TG/DTG profiles of: (a) $LiNbO_3$; (b) $NaNbO_3$; (c) $KNbO_3$.

Table 2 Desorbed oxygen for $ANbO_3$ (A = Li, Na, K) niobates

	Desorbed oxygen (mmol m^{-2})
$LiNbO_3$	0.027
$NaNbO_3$	0.029
$KNbO_3$	0.033

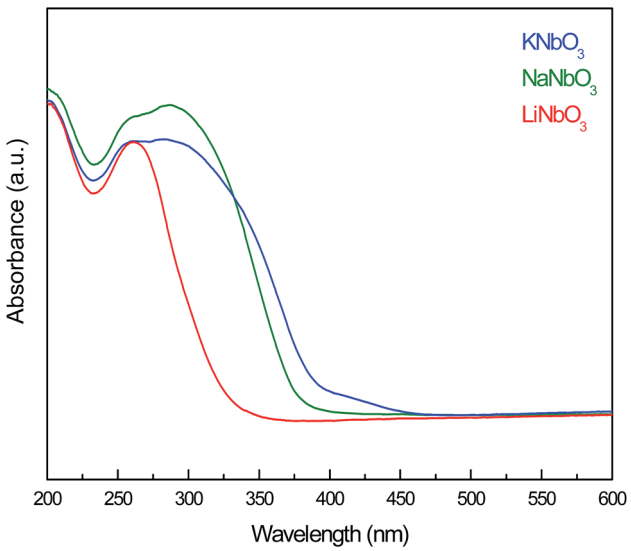

Fig. 3 DRS UV-Vis spectra of $ANbO_3$ (A = Li, Na, K) niobates.

by a broad band at 300–400 nm can be observed. It is noticeable that the broad peak at higher wavenumber appears as a shoulder for $KNbO_3$ and $NaNbO_3$. This feature can be attributed to a slightly distorted NbO_6 octahedra characteristic of perovskite-type oxides, as it has been previously reported by Turco *et al.*[40] and Zhu *et al.*[41] The difference in the DRS UV-Vis spectra of the $KNbO_3$ and $NaNbO_3$ perovskite-type oxides with regard to $LiNbO_3$ can be explained by the differences in the Nb–O–Nb angle within their crystalline structures. A stronger delocalization of the electronic wave functions can be achieved in the 180° of the Nb–O–Nb angle in the orthorhombic perovskite structure of $KNbO_3$ and $NaNbO_3$ compared to the nearly 125° of the Nb–O–Nb angle in a rhombohedral $LiNbO_3$ structure with a hexagonal axis.[42]

FTIR spectroscopy was employed to identify the nature of the segregated species present in the alkaline niobates and to verify the formation of the perovskite structure. The spectra of $LiNbO_3$, $NaNbO_3$ and $KNbO_3$ (Fig. 4) show a band at ~600 cm^{-1} attributed to the vibrational mode in the edge-shared NbO_6 octahedra.[43,44] In the case of $KNbO_3$, a shoulder at 850 cm^{-1} was assigned to an asymmetric enlargement of the B–O bond of the octahedral BO_6 structures indicative of the presence of the more crystalline perovskite structure. The band at 1495 cm^{-1} corresponds to the vibration of the CO_3^{2-} groups[45] and the band at 3600 cm^{-1} is assigned as the enlargement of the O–H bond in water. As it can be observed, $LiNbO_3$ has the cleanest surface structure and $KNbO_3$ the largest amount of segregated phases,

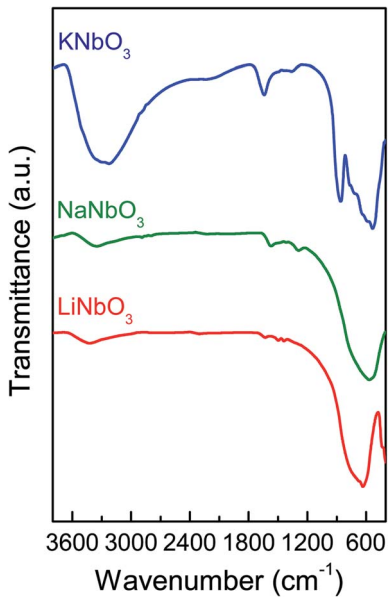

Fig. 4 FTIR spectra of $ANbO_3$ (A = Li, Na, K) niobates.

identified as CO_3^{2-} groups, also confirmed by XRD. In summary, the FTIR characterization provides strong evidence of crystalline phase formation for $LiNbO_3$, $NaNbO_3$ and $KNbO_3$.

3.2. Catalytic activity

Table 3 shows the conversion (mol%) obtained in the catalytic oxidation of DPS by the Li, Na and K niobates after 60 min of reaction time. It was observed that $KNbO_3$ has a higher degree of conversion followed by $NaNbO_3$ and $LiNbO_3$, indicating an increase in DPS oxidation down the alkaline group. The selectivity of DPS oxidation to prepare the sulfoxide (>95 mol%) is noticeably larger for these alkaline niobates, with sulfone (<5 mol%) as the only by-product observed. The larger catalytic activity of $KNbO_3$ can be related to the formation of surface oxygen-containing complexes in nano-sized particles, as previously reported by Zhang *et al.*[46] for K-substituted lanthanum perovskites. According to Escalona *et al.*[47] the highly symmetric cubic perovskite structures, similar to the perovskite structure with A and B-site vacancies, does not improve the catalytic activity. The orthorhombic and rhombohedral structures are the most appropriate structures for perovskite-type oxides, *i.e.*, as catalysts in catalytic combustion reactions.[47] On the other hand, despite the different atomic number, Na and Li niobates showed similar catalytic activity. This behavior could be attributed to the amount of desorbed oxygen, which in both of these niobates is similar as shown in the O_2-TPD results. Ivanov *et al.*[48] have demonstrated that excess oxygen in the rhombohedral perovskite structure enhances the availability and reactivity of oxygenated species on the catalytic surface due to weaker oxygen binding in this structure. Thus, $LiNbO_3$ may increase its catalytic activity due to the hexagonal rhombohedral structure, as demonstrated by XRD, equaling the activity of $NaNbO_3$.

To obtain a better correlation of the catalytic activity with the structural behavior of these materials, a kinetic study of the

Table 3 Conversion, selectivity and kinetic parameters of DPS oxidation with $ANbO_3$ (A = Li, Na, K) niobates[a]

Catalysts	Conversion (mol%)	Selectivity (mol%)		E_a (kJ mol^{-1})	k (10^{-2}) (min^{-1})	r_0 (10^{-3}) (mol g^{-1} min^{-1})
		Sulfoxide	Sulfone			
$LiNbO_3$	55.1	96.2	3.8	5.9	4.5	9.1
$NaNbO_3$	55.4	96.1	3.9	5.8	3.8	7.6
$KNbO_3$	77.1	94.9	5.1	3.0	5.5	11.0

[a] Reaction conditions: sulfide (4.0 mmol), 35% (w/v) H_2O_2 (4.0 mmol). Solvent: acetonitrile. Reaction time: 60 min. Catalyst amount: 20 mg. Temperature: 60 °C.

oxidation of DPS was performed. The suitable fit of the experimental data with a pseudo first order reaction, allowed us to determine the global pseudo first order constant and the initial reaction rate. The apparent activation energy (E_a) was calculated using the Stationary Point Method.[49] The obtained values are listed in Table 3 and in all cases the correlation coefficients were higher than 0.9. The global constant (k) and initial reaction rate (r_0) resulted similar for the $LiNbO_3$ and $NaNbO_3$ which agree with the catalytic behavior observed, and a higher value was obtained for the $KNbO_3$, reflected in a higher final DPS conversion. The estimated apparent activation energy values are much lower than those reported by Trikalitis and Pomonis[50] for perovskites in the reaction of propylene production. This important finding also supports the potential use of these alkaline niobates as catalysts for sulfide oxidation.

To determine the optimal reaction conditions, the most active niobate, $KNbO_3$ was selected to evaluate different reaction parameters. Firstly, the effect of the catalyst amount was studied and the obtained results are presented in Fig. 5.

At 60 min of reaction, DPS conversion values increases significantly from 54.0% to 77.1% when the catalyst mass increases from 10 to 20 mg. An increased concentration of $KNbO_3$ decreases degree of conversion with almost no changes in the sulfoxide selectivity (>94%), indicative of a similar reaction mechanism.[51] The optimal weight of catalyst can be explained considering the reports of Choudhary *et al.*[52] and Qi *et al.*[53] who indicate that at higher catalyst loading, hydrogen peroxide decomposition rates also increase, according to reaction (1).

$$H_2O_2 \rightarrow H_2O + 0.5O_2 \quad (1)$$

Considering that H_2O_2 decomposition and DPS oxidation occur simultaneously, the decreased availability of the oxidant explains the decrease in conversion level when the catalyst loading is raised to 20 mg. The non-catalytic reaction carried out under similar reaction conditions indicates a very low conversion rate, obtaining a final conversion of 5 mol% after 60 min.

The nature of the solvent is important on the reaction outcome, reaction kinetics and product selectivity, as previously reported by Corma *et al.*[54] The effect of the solvent was studied using $KNbO_3$, the better catalyst for the oxidation of DPS, using different protic and aprotic solvents. The DPS conversion (mol%) as a function of the solvent dielectric constant shown in Fig. 6 indicates a close relationship of sulfide conversion with solvent polarity, with no dependence on the aproticity or proticity of the solvent. This behavior indicates an increase in substrate concentration at the catalytic surface as the polarity of the solvent increases, as previously reported by Saux and Pierella.[55] The low conversion of DPS in *n*-hexane is due to the low miscibility of H_2O_2 in low polarity organic solvents.

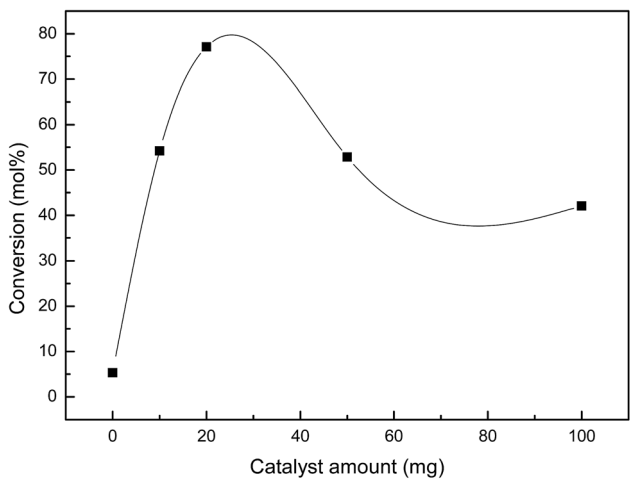

Fig. 5 Effect of catalyst weight on DPS conversion for $KNbO_3$ (reaction conditions: R = 1. Temperature: 60 °C. Reaction time: 60 min).

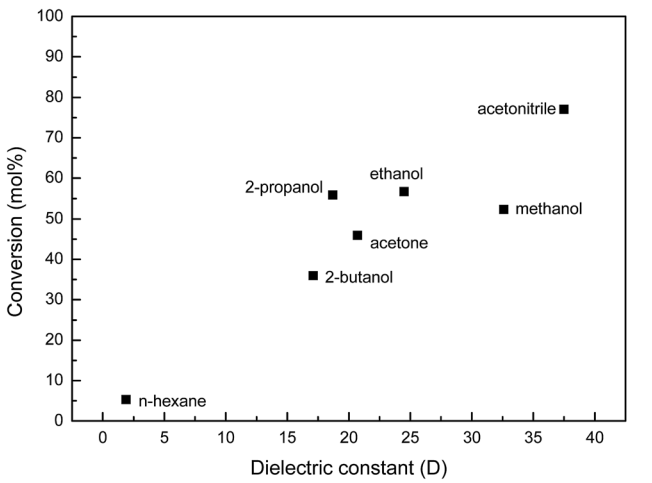

Fig. 6 Effect of solvent nature on DPS conversion for $KNbO_3$ (reaction conditions: R = 1. Catalyst amount: 20 mg. Temperature: 60 °C. Reaction time: 60 min).

To study the effect of the nature of the oxidant, *tert*-butyl hydroperoxide (TBHP) was selected to compare with the environmental friendly and extensively used hydrogen peroxide. Under similar experimental conditions, it was found that using TBHP as the oxidant results in a DPS conversion level decrease from 77.1 to 11.9 mol% and the dipropyl sulfoxide (the product of interest) selectivity decreases from 94.9 to 83.8%. Moreover, considering that H_2O_2 produces only water and TBHP more toxic by-products, we confirmed that hydrogen peroxide is the most attractive and environmental friendly oxidant.

The effect of the reaction temperature on $KNbO_3$ activity in DPS oxidation using a stoichiometric sulfide/oxidant molar ratio is shown in Fig. 7. A noticeable increase in conversion is observed up to 60 °C, and decreases at 80 °C. With regard to selectivity, at lower reaction temperatures the major product was sulfoxide; however, when the temperature was increased, the sulfoxide product decreased whereas sulfone production increased. At room temperature the DPS conversion was only 12.3% and increased to 43.4 and 77.1% as the temperature increased to 40 °C and 60 °C, respectively, with almost no change in sulfoxide selectivity (>94%). At 80 °C DPS conversion was slightly lower due to hydrogen peroxide consumption in a parallel auto-decomposition reaction (reaction (1)) that is favored at higher temperatures.

The recycled catalyst activity is an attractive property to reduce process costs and to follow environmental regulations. Again, $KNbO_3$ was selected to evaluate the reusability of these materials. The recycling study was carried out by filtration of the catalyst after the reaction was finished; followed by calcination in air at 500 °C for 8 h to remove residual organic species that could be adsorbed on the catalyst surface. The catalyst recycling was carried out four times under the same reaction conditions, and the conversion (mol%) of DPS as a function of the cycle is shown in Fig. 8.

A slight decrease is observed between the first and second reaction cycle with the conversion level remaining unchanged up to the fourth cycle. This behavior could be an evidence of leaching of some active species after the first use, a finding supported in a report by Mutreja *et al.*[56] that shows that some active potassium species could leach from impregnated potassium catalysts. To evaluate this hypothesis, the oxidation with fresh catalyst was performed and after 10 min of reaction time, the catalyst was completely removed *via* filtration and the reaction system was left to continue reacting for 60 additional minutes. Afterwards, DPS conversion increases only in 13.4 mol%. This result confirms the previous hypothesis of active species lixiviation during the first use of the catalyst and there are responsible for the observed homogeneous behavior. Based on these results, it is proposed that some potassium species that have remained segregated post-$KNbO_3$ synthesis are not embedded in the crystalline structure and could leach upon contact with a high dielectric constant solvent, such as acetonitrile, a solvent with a high dielectric constant that can solubilize ionic potassium species.

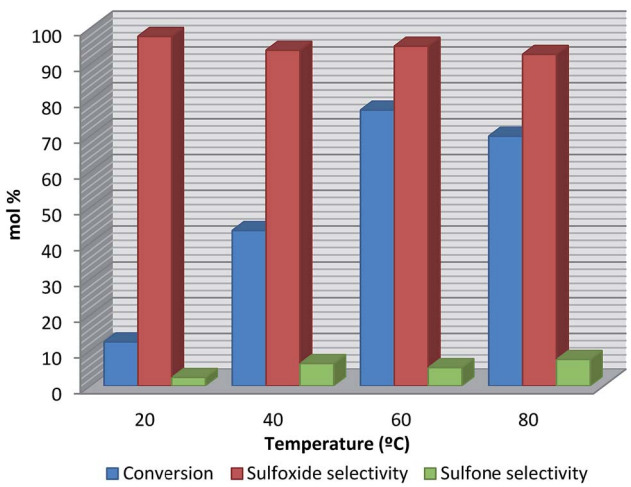

Fig. 7 Effect of reaction temperature on DPS conversion for $KNbO_3$ (reaction conditions: $R = 1$. Catalyst amount: 20 mg. Reaction time: 60 min).

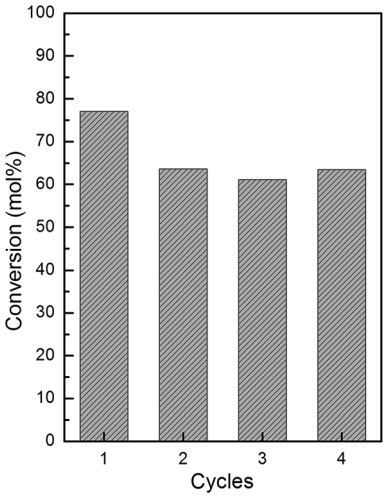

Fig. 8 Reuse cycles for $KNbO_3$ (reaction conditions: $R = 1$. Catalyst amount = 20 mg. Temperature: 60 °C. Reaction time: 60 min).

To gain a deeper insight of this catalytic oxidation and based on our interpretation of the experimental results and the identification of the oxidant products, simplified reaction steps are proposed for the catalytic DPS oxidation by $KNbO_3$ (Scheme 1). It has been previously reported[46,57] that the catalytic activity of perovskite-type catalysts for soot combustion is related to surface oxygen species, which migrate from within the perovskite structure to form surface oxygen-containing complexes in nanosized particles. Based on this statement, the catalytic activity for DPS conversion can be related to these superficial oxygen species. We propose that the sulfur atom of the sulfide generates a nucleophilic attack to an electrophilic center producing the corresponding sulfoxide and an oxygen vacancy, as previously reported.[11] Therefore, the large amount of desorbed oxygen obtained in the O_2-TPD experiments can be associated with the highest catalytic activity for $KNbO_3$, a perovskite-type oxide. The importance of desorbed oxygen from the surface of the catalysts for oxidation catalytic reactions was also analyzed by G. Pecchi *et al.*[58] and Fino *et al.*[59] Further, hydrogen peroxide restores the oxygen in the perovskite structure and generates water as

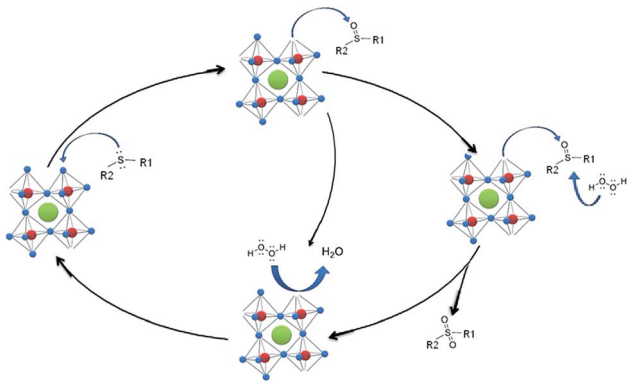

Scheme 1 Simplified reaction pathway for the oxidation of a sulfide to the corresponding sulfoxide and sulfone in an aqueous medium using hydrogen peroxide as the oxidant on a potassium niobate perovskite-type oxide.

by-product. The sulfoxide can be the final product, or generates the corresponding sulfone. The sulfone formation involves the interaction of the sulfoxide with the niobate by nucleophilic attack through the oxygen of the sulfoxide, by an H_2O_2 nucleophilic attack *via* a S_N2 mechanism.[60,61]

4. Conclusions

All of the prepared alkaline niobates tested in this study show catalytic activity for sulfide oxidation in the presence of hydrogen peroxide as the oxidant. The observed activity depends mainly on the nature of the alkaline metal and is related to the formation of oxygen vacancies. The catalytic activity follows an atomic number dependent order, namely: $KNbO_3 > NaNbO_3 \sim LiNbO_3$. The global constant, reaction rate and apparent activation energy were determined and the obtained values agreed with the catalytic results. The highest catalytic activity was obtained for $KNbO_3$, which is mainly attributed to the large amount of desorbed oxygen, and the amount of electron delocalization that increases as the Nb–O–Nb angle approaches 180° and promotes sulfide oxidation. The optimal experimental reaction conditions for DPS oxidation were at 60 °C with H_2O_2 as the oxidant, 20 mg of catalyst and acetonitrile as the solvent. Additionally, $KNbO_3$ can be successfully used as an easily recyclable catalyst up to four times with minimal leaching of potassium species only during the first reaction cycle.

Acknowledgements

This manuscript was partially supported by projects UTN-PID 1275 and UTI3864TC. Leal Marchena, Saux and Pierella thank CONICET-Argentina. Pecchi and Dinamarca thank CONICYT (Fondecyt Grant 1130005).

References

1 H. Mokbel, F. Dumur, B. Raveau, F. Morlet-Savary, C. Simonnet-Jegat, D. Gigmes, J. Toufaily, T. Hamieh, J. P. Fouassier and J. Lalevee, *Tetrahedron*, 2016, DOI: 10.1016/j.tet.2016.03.057.
2 G. Pecchi, C. Campos and O. Peña, *Catal. Today*, 2011, **172**, 111–117.
3 C. Nico, T. Monteiro and M. P. F. Graça, *Prog. Mater. Sci.*, 2016, **80**, 1–37.
4 M. Manzo, F. Laurell, V. Pasiskevicius and K. Gallo, in *Nano-Optics for Enhancing Light-Matter Interactions on a Molecular Scale*, ed. B. D. Bartolo and J. Collins, Springer, Netherlands, 2013, pp. 421–422.
5 K. Wang and J. F. Li, *J. Adv. Ceram.*, 2012, **1**, 24–37.
6 B. R. Stanmore, J. F. Brilhac and P. Gilot, *Carbon*, 2001, **39**, 2247–2268.
7 C. Badini, G. Saracco, N. Russo and V. Specchia, *Catal. Lett.*, 2000, **69**, 207–215.
8 R. Grange, F. Dutto and A. Radenovic, *Niobates Nanowires: Synthesis, Characterization and Applications, Implement. Appl.*, InTech, 2011.
9 Q. P. Ding, Y. P. Yuan, X. Xiong, R. P. Li, H. B. Huang, Z. S. Li, T. Yu, Z. G. Zou and S. G. Yang, *J. Phys. Chem. C*, 2008, **112**, 18846–18848.
10 J. He, A. Xu, L. Hu, N. Wang, W. Cai, B. Wang, J. Hu and Z. Li, *Powder Technol.*, 2015, **270**, 154–162.
11 C. Saux, C. Leal Marchena, R. Dinamarca, G. Pecchi and L. Pierella, *Catal. Commun.*, 2016, **76**, 58–61.
12 Y. Yuan and Y. Bian, *Tetrahedron Lett.*, 2007, **48**, 8518–8520.
13 K. Jeyakumar and D. K. Chand, *Tetrahedron Lett.*, 2006, **47**, 4573–4576.
14 M. M. Khodaei, K. Bahrami and M. Khedri, *Can. J. Chem.*, 2007, **85**, 7–11.
15 I. Sheikhshoaie, A. Rezaeifard, N. Monadi and S. Kaafi, *Polyhedron*, 2009, **28**, 733–738.
16 W. Al-Maksoud, S. Daniele and A. B. Sorokin, *Green Chem.*, 2008, **10**, 447–451.
17 M. Kirihara, J. Yamamoto, T. Noguchi, A. Itou, S. Naito and Y. Hirai, *Tetrahedron*, 2009, **65**, 10477–10484.
18 S. Choi, J.-D. Yang, M. Ji, H. Choi, M. Kee, K.-H. Ahn, S.-H. Byeon, W. Baik and S. Koo, *J. Org. Chem.*, 2001, **66**, 8192–8198.
19 F. Wang, C. Liu, G. Liu, W. Li and J. Liu, *Catal. Commun.*, 2015, **72**, 142–146.
20 H. M. Shen, W. J. Zhou, H. K. Wu, W. B. Yu, N. Ai, H. B. Ji, H. X. Shi and Y. B. She, *Tetrahedron Lett.*, 2015, **56**, 4494–4498.
21 M. Rahimizadeh, G. Rajabzadeh, S. M. Khatami, H. Eshghi and A. Shiri, *J. Mol. Catal. A: Chem.*, 2010, **323**, 59–64.
22 G. P. Romanelli, P. I. Villabrille, C. V. Cáseres, P. G. Vázquez and P. Tundo, *Catal. Commun.*, 2011, **12**, 726–730.
23 B. Zhang, S. Li, S. Yue, M. Cokoja, M. D. Zhou, S. L. Zang and F. E. Kühn, *J. Organomet. Chem.*, 2013, **744**, 108–112.
24 L. James, P. Martyn, S. Pandiaraju and A. K. Yudin, *J. Organomet. Chem.*, 2000, **603**, 98–104.
25 D. H. R. Barton, W. Li and J. A. Smith, *Tetrahedron Lett.*, 1998, **39**, 7055–7058.
26 C. O. Kinen, L. I. Rossi and R. H. de Rossi, *Appl. Catal., A*, 2006, **312**, 120–124.
27 N. M. Okun, J. C. Tarr, D. A. Hilleshiem, L. Zhang, K. I. Hardcastle and C. L. Hill, *J. Mol. Catal. A: Chem.*, 2006, **246**, 11–17.

28 G. P. Romanelli, G. P. Vázquez and P. Tundo, *Synlett*, 2005, **1**, 75–78.
29 M. Kirihara, J. Yamamoto, T. Noguchi and Y. Hirai, *Tetrahedron Lett.*, 2009, **50**, 1180–1183.
30 A. Shaabani and A. H. Rezayan, *Catal. Commun.*, 2007, **8**, 1112–1116.
31 L. H. Wang, D. R. Yuan, X. L. Duan, X. Q. Wang and F. P. Yu, *Cryst. Res. Technol.*, 2007, **42**, 321–324.
32 S. Yao, F. Zheng, H. Liu, J. Wang, H. Zhang, T. Yan, J. Wu, Z. Xia and X. Qin, *Cryst. Res. Technol.*, 2009, **44**, 1235–1240.
33 N. Russo, S. Furfori, D. Fino, G. Saracco and V. Specchia, *Appl. Catal., B*, 2008, **83**, 85–95.
34 N. M. Russo, D. Fino, G. Saracco and V. Specchia, *J. Catal.*, 2005, **229**, 459–469.
35 Y. Wang, J. Zhu, L. Zhang, X. Yang, L. Lu and X. Wang, *Mater. Lett.*, 2006, **60**, 1767–1770.
36 E. R. Camargo, M. Popa and K. Kakihana, *Chem. Mater.*, 2002, **14**, 2365–2368.
37 T. Ozawa, *J. Therm. Anal.*, 1970, **2**, 301–324.
38 T. Ozawa, *J. Therm. Anal.*, 1975, **7**, 601–617.
39 J. Zhu, Z. Zhao, D. Xiao, J. Li, X. Yang and Y. Wu, *J. Mol. Catal. A: Chem.*, 2005, **238**, 35–40.
40 R. Turco, A. Aronne, P. Carniti, A. Gervasini, L. Minieri, P. Pernice, R. Tesser, R. Vitiello and M. Di Serio, *Catal. Today*, 2015, **254**, 99–103.
41 H. Zhu, Z. Zheng, X. Gao, Y. Huang, Z. Yan, J. Zou, H. Yin, Q. Zou, S. H. Kable, J. Zhao, Y. Xi, W. N. Martens and R. L. Frost, *J. Am. Chem. Soc.*, 2006, **128**, 2373–2384.
42 G. Blasse and L. G. J. De Haart, *Mater. Chem. Phys.*, 1986, **14**, 481–484.
43 N. Belmokhtar, R. Brahimi, R. Nedjar and M. Trari, *Mater. Sci. Semicond. Process.*, 2015, **39**, 433–440.
44 M. Tatsumisago, A. Hamada, T. Minami and M. Tanaka, *J. Non-Cryst. Solids*, 1983, **56**, 423–428.
45 M. A. L. Nobre, E. Longo, E. R. Leite and V. Arela, *J. Mater. Sci. Lett.*, 1996, **28**, 215–220.
46 R. Zhang, N. Lou, B. Chen and S. Kaliaguine, *Energy Fuels*, 2010, **24**, 3719–3726.
47 N. Escalona, S. Fuentealba and G. Pecchi, *Appl. Catal., A*, 2010, **381**, 253–260.
48 D. V. Ivanov, L. G. Pinaeva, E. M. Sadovskaya and L. A. Isupova, *Kinet. Catal.*, 2011, **52**, 401–408.
49 B. Jankovic, B. Adnađević and S. Mentus, *Chem. Eng. Sci.*, 2008, **63**, 567–575.
50 P. N. Trikalitis and P. J. Pomonis, *Appl. Catal., A*, 1995, **131**, 309–322.
51 M. R. Maurya, A. K. Chandrakar and S. S. Chand, *J. Mol. Catal. A: Chem.*, 2007, **274**, 192–201.
52 V. R. Choudhary, N. S. Patil, N. K. Chaudhari and S. K. Bhargava, *Appl. Catal., A*, 1995, **131**, 309–322.
53 B. Qi, X. H. Lu, D. Zhou, Q. H. Xia, Z. R. Tang, S. Y. Fang, T. Pang and Y. L. Dong, *J. Mol. Catal. A: Chem.*, 2010, **322**, 73–79.
54 A. Corma, P. Esteve and A. Martínez, *J. Catal.*, 1996, **161**, 11–19.
55 C. Saux and L. Pierella, *Appl. Catal., A*, 2011, **400**, 117–121.
56 V. Mutreja, S. Singh and A. Ali, *Renewable Energy*, 2014, **62**, 226–233.
57 Z. Li, M. Meng, F. Dai, T. Hu, Y. Xie and J. Zhang, *Fuel*, 2012, **93**, 606–610.
58 G. Pecchi, B. Cabrera, E. J. Delgado, X. García and R. Jimenez, *Appl. Catal., A*, 2013, **453**, 341–348.
59 D. Fino, N. Russo, G. Saracco and V. Specchia, *J. Catal.*, 2003, **217**, 367–375.
60 R. Frenzel, A. G. Sathicq, M. N. Blanco, G. P. Romanelli and L. R. Pizzio, *J. Mol. Catal. A: Chem.*, 2015, **403**, 27–36.
61 A. Chellamani and S. Harikengaram, *J. Mol. Catal. A: Chem.*, 2006, **247**, 260–267.